Negative ion destruction by O(^{3}P) atoms and O$_2$($a\,^1\Delta_g$) molecules in an oxygen plasma

S G Belostotsky[1], D J Economou[2], D V Lopaev[1] and T V Rakhimova[1]

[1] Skobeltsyn Nuclear Physics Institute of Lomonosov Moscow State University, Moscow 119992, Russia
[2] Plasma Processing Laboratory, Department of Chemical Engineering, University of Houston, TX 77204-4004, USA

Abstract
Laser photodetachment was used to investigate the dynamics of negative ion density in the positive column of a pure oxygen dc glow discharge over a range of pressure (0.1–5 Torr) and current density (2–40 mA cm^{-2}). Upon discharge current modulation, the negative ion O$^-$ concentration decayed with the characteristic loss times of oxygen O(^{3}P) atom and metastable oxygen O$_2$($a\,^1\Delta_g$) molecule concentrations over a wide range of discharge parameters. To determine the rate constants of negative ion loss by reaction with these species, the dynamics of O(^{3}P) atoms and O$_2$($a\,^1\Delta_g$) molecules was investigated using time-resolved actinometry and IR spectroscopy at 1.27 μm, respectively. At pressures greater than ∼0.5 Torr the attachment–detachment dominated regime of the oxygen discharge was realized and the main negative ion was O$^-$. Under these conditions, electron attachment to O$_2$ molecules to produce O$^-$ was compensated by detachment of O$^-$ with O(^{3}P) and O$_2$($a\,^1\Delta_g$). The rate constants of O$^-$ detachment with O(^{3}P) atoms (O$^-$ + O(^{3}P) → O$_2$ + e: $k_d^O = (2.3 \pm 0.5) \times 10^{-10}$ cm^3 s^{-1}) and singlet O$_2$($a\,^1\Delta_g$) molecules (O$^-$ + O$_2$($a\,^1\Delta_g$) → products + e: $k_d^\Delta = (1.9 \pm 0.4) \times 10^{-10}$ cm^3 s^{-1}), were determined in the plasma itself for the first time.

1. Introduction

Electronegative plasmas in gases such as CF$_4$, C$_2$F$_6$, C$_3$F$_8$, SF$_6$, Cl$_2$ or O$_2$ are used widely in various technologies, especially in microelectronics [1]. Negative ions play an important role in plasmas of electronegative gases. They participate in a variety of chemical reactions (e.g. associative detachment with radicals, metastable atoms and molecules) affecting the charge balance and in turn the electric field and electron energy distribution function (EEDF). Furthermore, negative ions play an active role in electronegative plasma polymerization and dusty plasma formation. Finally, in pulsed plasmas through electronegative gases, the transition from an electron-dominated plasma to an ion–ion plasma depends on negative ion chemistry and dynamics [2, 3]. Therefore,

knowledge of negative ion kinetics is of interest to both fundamental and applied research.
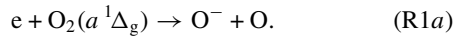
Negative ion production and loss and the rate constants of these processes are considered to be most important for describing the kinetics of electronegative plasmas. Negative ions may be destroyed in the plasma volume by associative detachment with neutral radicals and metastable molecules. When the negative ion concentration in such plasmas is significant, i.e. when $n^-/n_e > 1$ (n^- and n_e are concentrations of negative ions and electrons, respectively), negative ion reactions can have a substantial effect on plasma parameters (charge composition, EEDF) and plasma process outcome. Therefore, it becomes necessary to study negative ion detachment with reactive neutrals and to determine the corresponding reaction rate constants.

In this work a pure oxygen plasma was investigated. In addition to being of practical interest, the oxygen plasma can be thought of as a 'model' electronegative plasma in the sense that basic processes involving negative ions are also applicable to other electronegative discharges. At the same time there is a wealth of information (cross-sections, rate constants of important reactions) as a result of past experimental and theoretical studies of O_2 plasmas, which greatly facilitates basic investigations. Moreover, oxygen plasmas are 'clean', without complications by film deposition, and the gas is easy to handle.

The main process of negative ion production in a pure oxygen plasma at $0.05 < pR < 50$ Torr cm (p—pressure, R—tube radius as the characteristic plasma length) is dissociative attachment of electrons to oxygen molecules,
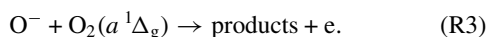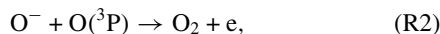
$$e + O_2 \rightarrow O + O^-. \tag{R1}$$

Dissociative attachment of electrons to metastable singlet oxygen $O_2(a\,^1\Delta_g)$ can also be important,

$$e + O_2(a\,^1\Delta_g) \rightarrow O^- + O. \tag{R1a}$$

The concentration of singlet oxygen in the plasma can be significant (mole fraction ~ 0.1). The rate constant of reaction (R1a), which is almost independent of E/N in the range of interest, can be four times greater than that of reaction (R1). Thus, reaction (R1a) can make a noticeable contribution to O^- production.

Since the ambipolar electric field traps negative ions in the plasma volume, the negative ion concentration in the plasma sheath is extremely low. The negative ion concentration profile in the bulk plasma depends mainly on the ratio of tube radius R to the characteristic detachment length Λ_{det}. In oxygen plasmas, at $pR > 0.3$ Torr cm, $R \gg \Lambda_{det} \approx \sqrt{D_a/\nu_{det}}$, that is, $\nu_{det}\tau_{ad} > 1$ [4, 5], where D_a—coefficient of ambipolar diffusion, τ_{ad}—characteristic time of ambipolar diffusion and ν_{det}—frequency of negative ion detachment with oxygen atoms and excited metastable molecules. Under the same pR condition, the tube radius is also greater than the characteristic length of dissociative attachment Λ_{att} ($R \gg \Lambda_{att} \approx \sqrt{D_a/\nu_{att}}$, that is, $\nu_{att}\tau_{ad} > 1$, where $\nu_{att} = k_{att}O_2$—frequency of dissociative attachment). Therefore, the discharge operates in the so-called 'attachment–detachment' dominated regime, in which the production of negative ions by attachment is balanced by their loss through detachment. In this regime the spatial *profile* of electron density coincides with that of the negative ion density i.e. $n^-(r)/n_e(r) \cong$ constant [5–12]). When $pR < 0.3$ Torr cm, $\nu_{att}\tau_{ad} < 1$ and the attachment length Λ_{att} is greater than the tube radius ($\Lambda_{att} > R$). In this case, the spatial profiles of negative ion and electron concentrations are different, and the plasma may stratify into an ion–ion core and an electron–ion periphery [4, 13, 14].

In the attachment–detachment regime of the oxygen discharge, the main processes of O^- destruction are the associative detachment with oxygen atoms in the ground state $O(^3P)$ and the singlet metastable molecules $O_2(a\,^1\Delta_g)$:

$$O^- + O(^3P) \rightarrow O_2 + e, \tag{R2}$$

$$O^- + O_2(a\,^1\Delta_g) \rightarrow products + e. \tag{R3}$$

Although oxygen plasmas have been studied for a long time, there is still controversy over the rate constants of these detachment reactions, especially reaction (R3) involving singlet oxygen molecules $O_2(a\,^1\Delta_g)$. For example, the values of the corresponding rate constant k_3 reported in two different studies differ by one order of magnitude [15, 16]. Modellers of the oxygen discharge are then faced with the dilemma of choosing a value of k_3 in between the reported values, in such a way as to 'fit' simulation predictions to the experimental data. Such 'fitting', however, diminishes the value of the modelling effort.

In this work negative ion detachment with $O(^3P)$ atoms and $O_2(a\,^1\Delta_g)$ molecules in the positive column of a pure oxygen dc glow discharge was studied in detail. The rate constants of these processes were determined, for the first time, in the plasma itself.

2. Experiment

2.1. Experimental principles

A dc glow discharge in a long cylindrical tube (12 mm-inside diameter) was used for experimental work (figure 1). The distance between the electrodes was 490 mm. A special feature of this configuration is the spatial homogeneity of the discharge along the tube axis in the positive column region. This feature turned out to be very convenient for both experimental and theoretical studies. Experiments were carried out in pure oxygen for pressures in the range 0.1–5 Torr and current densities in the range 2–40 mA cm^{-2}.

As mentioned earlier, neglecting the plasma sheath, the radial profiles of electron and negative ion density coincide in the attachment–detachment regime [4, 14]. This provides an opportunity to perform accurate determination of negative ion density, averaged over the tube radius, using laser photodetachment. In the traditional application of this technique, negative ions are photodetached using laser radiation of the appropriate wavelength and the resulting electrons are measured using Langmuir probes or microwave interferometry [18–20]. Since it is very difficult to ascertain the size of the volume over which electrons are collected, accurate calibration of the probe or interferometer signal to obtain an absolute measure of the negative ion density is challenging. This can lead to significant and often uncontrolled measurement errors. To avoid such a problem in this work,
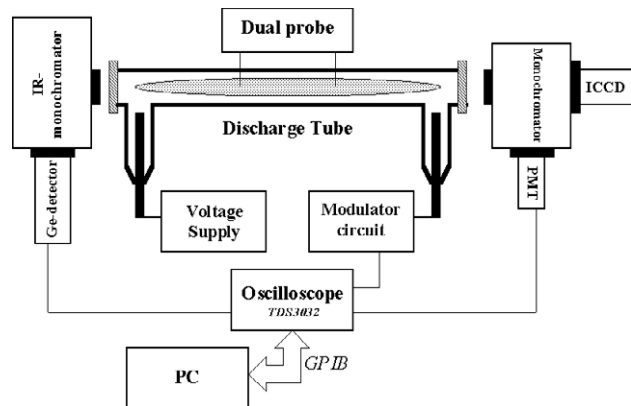

Figure 1. Schematic diagram of the experimental set-up used to investigate the dynamics of $O(^3P)$ and $O_2(a\,^1\Delta_g)$ concentrations.

the laser beam irradiated the whole cross-section of the discharge tube and the anode was used as the electron collecting probe. Therefore, the acquired signal was proportional to the cross-section average concentration of negative ions. In the attachment–detachment regime, in which the radial profiles of electron and negative ion concentrations 'coincide', the n^-/n_e ratio is independent of radial position and is equal to the cross-section average value.

However, since the negative ion loss is determined mainly by its detachment from the oxygen atoms and the singlet molecules, one should also measure the concentrations of these neutral species in plasma. Atomic oxygen can be lost by recombination on the plasma containing wall and singlet molecules can deactivate on this wall. The loss probabilities for atoms γ_O and singlet oxygen molecules γ_Δ on glass and fused quartz are quite low, $\gamma_O \approx 10^{-3}$ and $\gamma_\Delta \approx 10^{-4}$ [21, 22]. For that reason, the radius of the discharge tube ($R = 0.6$ cm) is much less than the characteristic length of $O(^3P)$ or $O_2(a\,^1\Delta_g)$ loss, $\Lambda_{loss} \approx 2.4\sqrt{D\tau_{loss}} \sim 10$–100 cm ($D$— diffusion coefficient, τ_{loss}—wall loss lifetime). Therefore, wall loss of these species occurs in the kinetically controlled regime (fast diffusion) and the radial distribution of both atoms and singlet molecules coincides with that of $O_2(X\,^3\Sigma_g^-)$ in the ground state (determined by the radial gas temperature profile). It follows that the concentration ratios [O]/[O_2] and [$O_2(a\,^1\Delta_g)$]/[O_2] (where [O], [$O_2(a\,^1\Delta_g)$] and [O_2] are the concentrations of oxygen atoms, molecules in the singlet state and molecules in the ground state, respectively) as well as n^-/n_e do not depend on radial position. Therefore, one may use the corresponding cross-section average values of these ratios. In conclusion, in the range $0.3 < pR < 10$ Torr cm, the experimental arrangement and techniques used in this work are well-suited to quantitatively investigating the associative detachment reactions (R2) and (R3).

The tube wall temperature was monitored at two axial locations using chromel–alumel thermocouples. The gas temperature T_g at the discharge axis was measured using the P-branch of the $O_2(b\,^1\Sigma_g^+, v = 0) \rightarrow O_2(X\,^3\Sigma_g^-, v = 0)$ rotational band at $\lambda = 762$–770 nm. An example of such a measurement is shown in figure 2. The fine structure of the P-branch (QP and PP branches) was not resolved. However, this should not influence the temperature measurements seriously (error less than 7%) [17]. The gas temperature increases linearly with power deposited per centimetre of positive column (figure 2), in agreement with [17]. This allows one to determine the gas temperature on axis, from measurements of electric field and discharge current (e.g. power per unit length). Having measured the wall temperature and assuming a parabolic profile, the gas temperature was determined as a function of radial position. This was, in turn, used to find the total neutral gas density as a function of position, knowing the total pressure and applying the ideal gas law.

When the O^- density is determined by the balance between dissociative attachment (reactions (R1) and (R1a)) and associative detachment (reactions (R2) and (R3)), the following expression may be derived:

$$\frac{[O^-]}{n_e} = \frac{k_{att}}{k_2([O(^3P)]/[O_2]) + k_3([O_2(a\,^1\Delta_g)]/[O_2])}, \quad (1)$$
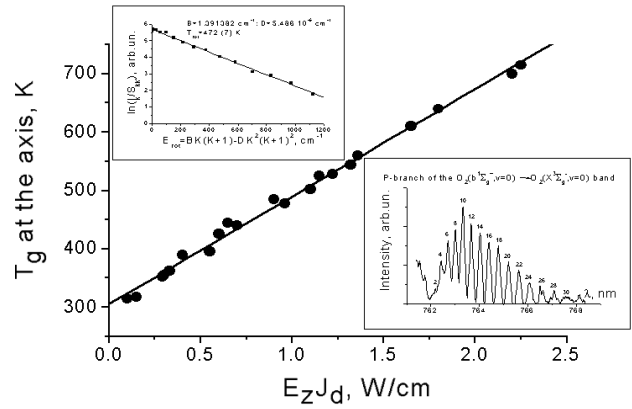
Figure 2. Gas temperature at the tube axis as a function of power per centimetre of positive column. E_z—axial electric field, J_d—discharge current. Upper left inset—example of measurement of oxygen rotational temperature by plotting the logarithm of the ratio $I_k/S_{kk'}$ (I_k—intensity of the rotational line, $S_{kk'}$— Heln–London factor) against the rotational energy of the oxygen molecule ground state; $p = 3$ Torr, $J_d = 25$ mA, $E_z J_d = 1.14$ W cm^{-1}, $T_{rot} = 472 \pm 7$ K. Lower right inset—rotational structure of the P-branch of the $O_2(b\,^1\Sigma_g^+, v = 0) \rightarrow O_2(X\,^3\Sigma_g^-, v = 0)$ band.

where k_{att}—total rate constant of dissociative attachment, i.e. $k_{att} = k_{att}^X + k_{att}^\Delta(O_2(a\,^1\Delta_g)/O_2)$, k_{att}^X—rate constant of dissociative attachment to O_2 molecules in the ground state, k_{att}^Δ—rate constant of dissociative attachment to $O_2(a\,^1\Delta_g)$, [O^-]—negative ion concentration, k_2 and k_3—rate constants of O^- loss on $O(^3P)$ atoms and $O_2(a\,^1\Delta_g)$ molecules, respectively. Neglecting the possible variation of k_{att} (caused by variation of E/N) along the tube radius, one can see that all quantities in equation (1) (concentration ratios and rate constants) are independent of the radial coordinate. By measuring the concentration ratios and knowing k_{att}, k_2 and k_3 may thus be determined.

Discharge current modulation can be applied to separate the two dominant negative ion loss channels since the characteristic lifetimes of atoms and singlet molecules differ considerably. When a step change (square wave modulation) of the discharge current is applied, the neutral species concentrations (oxygen atoms and metastable molecules) reach their new steady state with a characteristic time depending on the loss process of the given species. Thus, the evolution of negative ion concentration with these characteristic times provides information about the rate of negative ion loss with $O(^3P)$ and $O_2(a\,^1\Delta_g)$. In this paper, time-resolved actinometry was used to investigate the atomic oxygen dynamics. The dynamics of singlet oxygen molecules was studied by IR emission spectroscopy at 1.27 μm.

2.2. Measurement of concentration and dynamics of atomic oxygen

Figure 1 is a schematic diagram of the experimental set-up to investigate the dynamics of $O(^3P)$ and $O_2(a\,^1\Delta_g)$ concentrations. Time-resolved actinometry (with Ar as the actinometer) was applied to measure the dynamics of atomic oxygen in the ground state [21]. The $O(3p\,^5P \rightarrow 3p\,^5S)$ at $\lambda = 777.1$ nm and $Ar(2p_1-1s_2)$ at $\lambda = 750.4$ nm transitions were used. These transitions are typical for oxygen atom

actinometry, when the contribution of dissociative excitation to the 777.1 nm emission is accounted for, based on the following formulae, valid for a stationary discharge [21, 23, 25, 26]:

$$\frac{[\text{O}(^3\text{P})]}{[\text{O}_2]} = C_\text{O}^\text{Ar} \frac{I_{777}}{I_{750}} - \frac{k_\text{de}^{\text{O}_2}}{k_\text{e}^\text{O}}, \qquad (2)$$

$$C_\text{O}^\text{Ar} = \frac{[\text{Ar}]}{[\text{O}_2]} \frac{h\nu_{nm} A_{nm}}{h\nu_{ij} A_{ij}} \frac{k_\text{e}^\text{Ar}}{k_\text{e}^\text{O}} \frac{\sum_j A_{ij} + \sum_q k_q^\text{O}[M_q]}{\sum_m A_{nm} + \sum_q k_q^\text{Ar}[M_q]}, \qquad (3)$$

where ν_{ij}, A_{ij} and ν_{nm}, A_{nm}—frequencies and Einstein's coefficients for oxygen and argon atoms, respectively; k_e^O and k_e^Ar—rate constants of electron impact excitation of emitting states O* and Ar*, respectively; $k_\text{de}^{\text{O}_2}$—rate constant of excited atom O* production by dissociative excitation of O_2 molecules; k_q^O and k_q^Ar—quenching rate constants of emitting states of atoms O* and Ar* by collisions with species q; I_{777} and I_{750}—emission line intensities of oxygen and argon atoms, respectively; [Ar], [O], $[\text{O}_2]$ and $[M_q]$—concentrations of Ar, O(^{3}P), O_2 and species q (in this case $M_q \approx \text{O}_2$).

The electron impact rate constants in equations (2) and (3) were calculated using a self-consistent model of a dc glow discharge in pure oxygen [14, 23–25]. The EEDF as a function of radial position was found self-consistently by a particle-in-cell/Monte-Carlo (PIC/MC) technique or by solving the non-local Boltzmann equation [14, 23–25]. Oxygen atoms and singlet oxygen molecules have long lifetimes, resulting in relatively high density of these species in the discharge, which can influence the electron density, electric field and EEDF via detachment reactions with negative ions. The non-locality of the EEDF appears to be important only at low pressures ($pR < 0.3$ Torr cm) for which the EEDF tail is strongly depleted because of kinetic losses of fast electrons to the wall [14, 24]. This was verified by measuring the radial distribution of the EEDF for a wide range of discharge parameters [24]. Such experiments confirmed the PIC–MC simulation used to calculate the EEDF. At the same time the non-local approach, based on finding the EEDF from the Boltzmann kinetic equation in the two-term approximation, turned out to be inapplicable near the wall at low values of pR, i.e. at high degrees of non-locality [24].

The non-locality of the EEDF significantly affects the rate constants of electron impact excitation [23] and dissociation [25] and hence the oxygen atom concentration. It also affects the excitation rate constants and emission intensities of oxygen and argon atoms. However, the *ratio* of excitation rate constants remained almost identical to that predicted by the local approach [23–25]. This finding makes it possible to use actinometry for measuring the atomic oxygen concentration in dc glow discharges even at low pressures, where the non-locality of the EEDF may be important. We have analysed available data on excitation cross-sections of argon and oxygen atoms including dissociative excitation [26–28]. The analysis of actinometric measurements in [26] agreed well with results from our models regarding ratios of emission intensities, excitation rate constants and oxygen atom density. Therefore, we used the excitation cross-sections proposed in [26]. Modulation of discharge current allows one to determine the contribution of dissociative excitation of O_2 to the intensity of the atomic oxygen emission line at 777 nm [21, 23]. The contribution of dissociative excitation turned out

to be competing with direct excitation only at low discharge currents (<5 mA, when the O/O_2 ratio is small) and/or at low pressures (<0.3 Torr, when the reduced electric field E/N is high).

In order to verify our experimental results, a set of measurements of oxygen atom concentration by resonant VUV absorption using the O($2p\,^3$P $\rightarrow$ $3p\,^3$S) transition ($\lambda = 130$ nm) was carried out. A surface wave discharge in He with a small ($\sim$1% by volume) amount of added oxygen was used as the VUV radiation source. The surface wave ('surfatron') discharge was maintained by a microwave generator ($f = 2.45$ GHz, $P = 30$–100 W) in a quartz tube (15 mm inside diameter). The dc oxygen discharge was placed between the VUV source and a VUV monochromator through MgF$_2$ windows. Unfortunately, the resolution of the VUV monochromator was too low to resolve the fine structure of the O-atom resonant line. Therefore, calibration of resonant absorption to obtain the absolute atom concentration was not realized. However, estimates of the O(^{3}P) density, obtained from the absorption in the wings of the lines, were in good agreement with the results of actinometric measurements. Nevertheless, the relative changes in O(^{3}P) density, as determined by VUV absorption, were the same as those found by actinometry for a wide range of discharge parameters, giving credence to the actinometric measurement of O(^{3}P) concentration. In order to further validate our data we conducted a combined experimental-simulation study of the dissociation balance in a dc oxygen discharge [25]. The loss rate of oxygen atoms was measured and the O_2 dissociation by electron impact was calculated based on the well accepted cross-sections. This investigation also allowed an indirect determination of the uncertainty ($\pm$20%) of the absolute value of the of O/O_2 ratio found actinometrically. Relative values of that ratio are expected to be more accurate.

The concentration ratio [O(^{3}P)]/[O_2] (a measure of the degree of gas dissociation) as a function of discharge current at different pressures is presented in figure 3(*a*). As mentioned above, this ratio does not depend on radial position because the radial profiles of O(^{3}P) atoms and O_2 molecules are identical, as determined by the gas temperature profile. The concentration ratio is a linear function of discharge current and depends weakly on pressure (the reduced electric field varies from $\sim$60 Td at 5 Torr to $\sim$320 Td at 0.1 Torr).

Figure 3(*a*) provided the atomic oxygen concentration in a stationary discharge. Discharge current modulation was applied to measure the time constant of O(^{3}P) surface recombination loss in the discharge [21, 23]. Upon a step change in the discharge current (15–20% increase of the current value), the time evolution of the change in atomic oxygen concentration [δO(^{3}P)](t) will be exponential, for a first-order process. The radiative lifetime of the O* and Ar* emitting states as well as the relaxation times of the EEDF and electron density are much shorter than the O-atom lifetime. Therefore, after a fast plasma relaxation, the time evolution of the actinometric signal is a direct measure of the time evolution of [δO(^{3}P)]. Possible variation of discharge parameters (e.g. electric field, current) caused by O-atom associative detachment with negative ions [14], should not affect the results since the O* emission is normalized by the Ar* emission in actinometry. It should also be mentioned
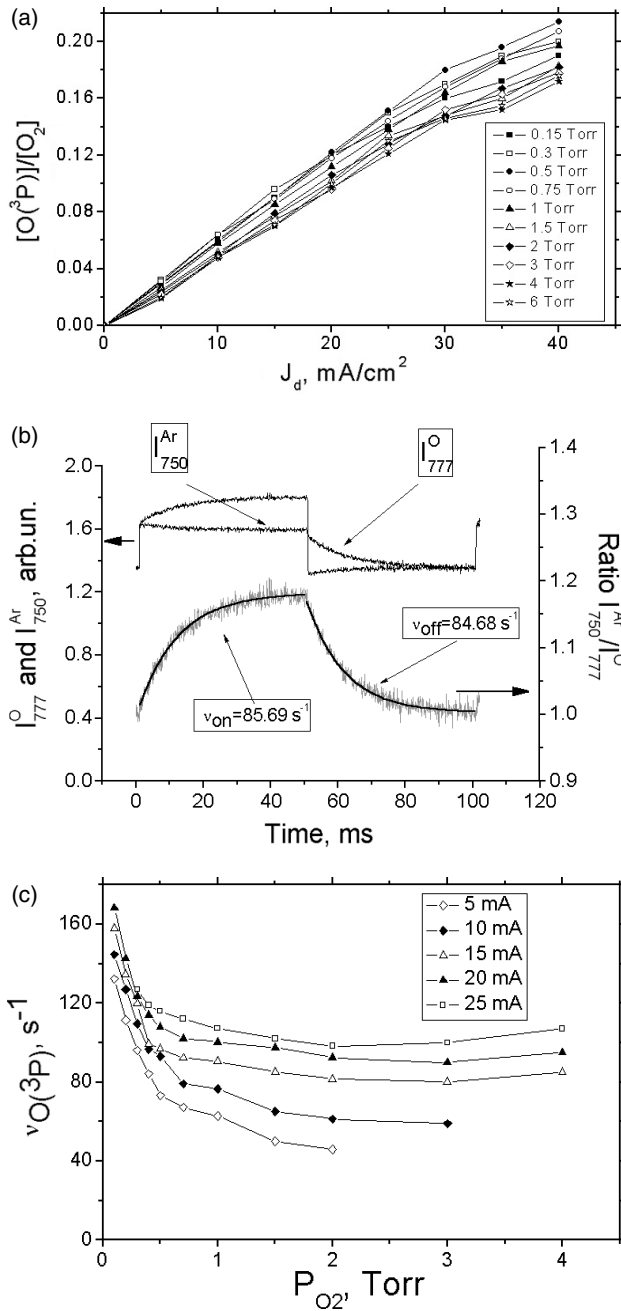
Figure 3. (*a*) [O(^{3}P)]/[O$_2$] ratio as a function of discharge current density at different oxygen pressures for stationary discharges. (*b*) Typical evolution of intensities of O (777 nm) and Ar (750 nm) emission lines and actinometric signal upon discharge current modulation. $p_{O_2} = 0.4$ Torr, $J_d^{max} = 10$ mA cm^{-2}, $\delta J_d = 2.2$ mA cm^{-2}. (*c*) Loss frequency of O-atoms as a function of pressure at different discharge currents.

that the current modulation depth should be small enough for the characteristic times of radical production and loss to be nearly equal. Otherwise, if the modulation depth is too large, gross perturbation of the system may occur involving multiple reaction channels of the species of interest.

If the contributions of both dissociative excitation of O* and background radiation at the emission band of the radical can be neglected, the relative change of atomic oxygen density

upon discharge modulation is given by,

$$1 + \frac{[\delta O](t)}{[O]_0} = \frac{1 + \delta I_O(t)/I_O^0}{1 + \delta I_{Ar}(t)/I_{Ar}^0}, \quad (4)$$

where index '0' refers to the initial values (before the step change). Thus, in order to represent the dynamics of the ratio $[\delta O](t)/[O]_0$ properly it is important to use the normalized emission, i.e. I_O/I_{Ar}. A typical time evolution of the discharge current, intensities of O (777 nm) and Ar (750 nm) emission lines and actinometric signal $S_O = (1 + \delta I_O/I_O^0)/(1 + \delta I_{Ar}/I_{Ar}^0)$ are presented in figure 3(*b*). An exponential fit of the signal growth and decay is also shown. The characteristic frequencies of O-atom growth and decay are quite similar, which reassures that the technique is applicable for measuring the loss frequency of oxygen atoms.

Figure 3(*c*) shows the O-atom loss frequency as a function of pressure at different discharge currents. Surface recombination processes depend on the density of active sites on the surface which can change as discharge conditions vary. This explains the dependence of surface recombination probability on pressure and current [21, 25, 29].

2.3. Measurement of concentration and dynamics of singlet oxygen

The concentration of oxygen in the first singlet state—O$_2$(a $^1\Delta_g$) was measured using IR spectroscopy. Emission at $\lambda = 1.27$ μm owing to the transition O$_2$(a $^1\Delta_g$, $v = 0$) → O$_2$(X $^3\Sigma_g^-$, $v = 0$), was recorded using a nitrogen-cooled Ge-detector, ADC 403. Emission was collected from both the axial end of the discharge tube (with an IR monochromator) and from the tube side through a narrow-band interference filter with $\Delta\lambda_{1/2} = 12$ nm (see figure 1). It should be emphasized that only the O$_2$(a $^1\Delta_g$, $v = 0$) → O$_2$(X $^3\Sigma_g^-$, $v = 0$) band was observed in the spectrum of pure oxygen discharge in the range 1200–1300 nm. To obtain absolute concentration measurements, calibration of O$_2$(a $^1\Delta_g$) intensity was performed with the help of a radiometer (EG&G 550-1) and a series of interference filters, which simulated the O$_2$(a $^1\Delta_g$, $v = 0$) → O$_2$(X $^3\Sigma_g^-$, $v = 0$) spectral band with accuracy better than 10%. The known Einstein's coefficients of the O$_2$(a $^1\Delta_g$, $v = 0$) → O$_2$(X $^3\Sigma_g^-$, $v = 0$) transition were used ($A = 2.2 \times 10^{-4}$ s^{-1} see [30, 31] and references therein). We have carried out independent calibrations of the O$_2$(a $^1\Delta_g$) concentration both from the axial end and from the side of the discharge tube. The two sets of data were identical to within ~10%. The total calibration error was estimated to be ±15%.

The concentration of O$_2$(a $^1\Delta_g$) as a function of pressure at different discharge currents is shown in figure 4(*a*). The singlet oxygen concentration saturates both with pressure and with discharge current. Under the experimental conditions, quenching on the tube wall and by electron impact are the main processes of O$_2$(a $^1\Delta_g$) destruction. Since the radiative lifetime of singlet oxygen is very long (~4500 s), greatly exceeding the quenching time, the evolution of O$_2$(a $^1\Delta_g$) emission intensity should follow the evolution of the O$_2$(a $^1\Delta_g$) concentration as the discharge current is modulated. A typical time evolution of the discharge current (step change) and the singlet oxygen concentration is presented in figure 4(*b*). The discharge current
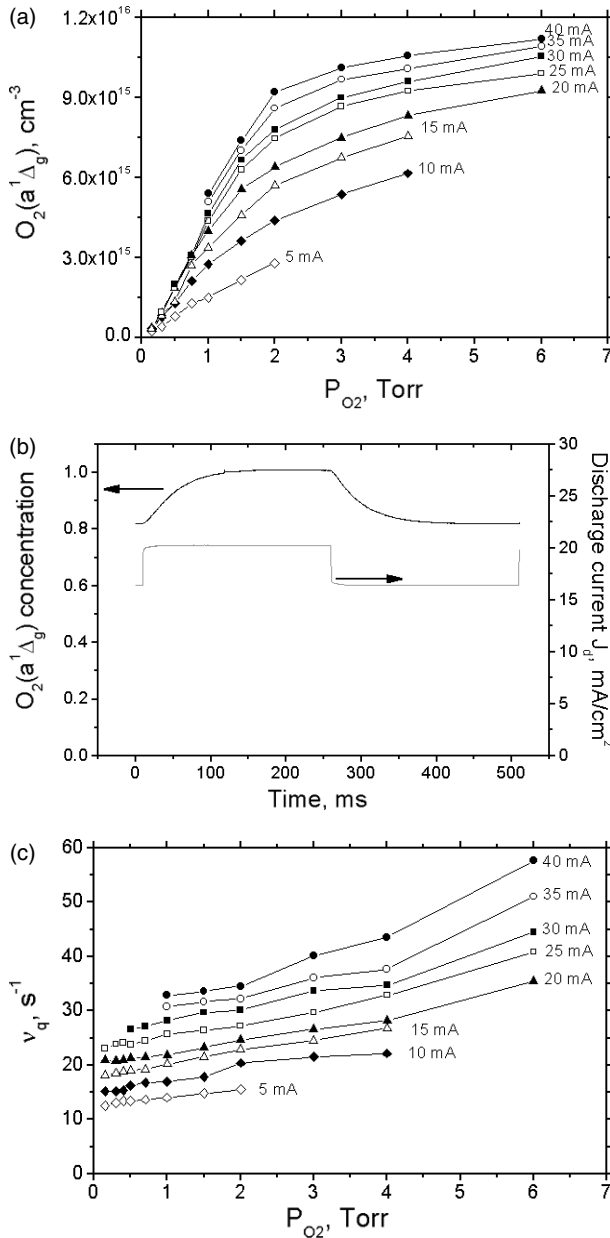
(a)

(b)

(c)

Figure 4. (*a*) Concentration of $O_2(a\,^1\Delta_g)$ as a function of pressure at different discharge currents in a stationary discharge. (*b*) Evolution of the discharge current and the singlet oxygen concentration for a modulated discharge with $p_{O_2} = 1.5$ Torr. (*c*) Frequency of singlet oxygen quenching as a function of pressure at different discharge currents.

reaches its new stationary value much faster than the $O_2(a\,^1\Delta_g)$ concentration, so the dynamics of singlet oxygen is determined solely by quenching. Exponential fits of the growth and decay of the $O_2(a\,^1\Delta_g)$ concentration, allow one to obtain the species quenching frequency. The quenching frequency is found to increase with the discharge current (figure 4(*c*)) since the electron density increases with current. The quenching frequency also increases with pressure at fixed current, again because the electron density increases, as a result of decreasing reduced electric field (and thus drift velocity).

2.4. Measurement of concentration and dynamics of negative ions

A schematic diagram of the laser photodetachment apparatus is presented in figure 5. KrF excimer laser radiation ($\lambda = 248.5$ nm, $\tau_{\text{pulse}} = 20$ ns and $f_{\text{rep}} = 5$ Hz) with a pulse energy up to 150 mJ entered through a quartz window from one axial end of the discharge tube. The laser pulse energy was measured at the other end of the tube by a Coherent Ultima LabMaster. The discharge current following a laser pulse was measured as the voltage across a $r = 50\,\Omega$ resistor, using a Digital Oscilloscope-Tektronix TDS 3032, connected with a PC via GPIB. The time evolution of the reduced field in the positive column was also measured using a dual probe technique (probe diameter 0.04 cm). The probe signal was recorded with an oscilloscope using a 5 MHz differential amplifier with large input resistance ($>10\,M\Omega$). The oscilloscope was synchronized with the laser pulse with the help of the Digital Delay Generator (PAR 9650A), which also triggered the modulator circuit. The overall experiment and data acquisition were controlled using LabVIEW.

The dynamics of discharge current and reduced electric field after a laser pulse are presented in figures 6(*a*) and (*b*), respectively. After a laser pulse, the discharge current increases abruptly before decaying rather slowly to its original level. The current jump is due to a sudden increase in electron density caused by laser photodetachment of negative ions. The electron current dominates in the positive column of the glow discharge. Therefore,

$$j_0 \propto n_e, \qquad \delta j = j_{\text{max}} - j_0 \propto n_{\text{pd}} = [O^-]_{\text{pd}}, \qquad (5)$$

where n_e, n_{pd} and $[O^-]_{\text{pd}}$ are electron, detached electron and detached negative ion concentration, respectively, all averaged over the tube cross-section. Also, j_0 is the initial discharge current and j_{max} is the current maximum, after the laser pulse.

The current relaxation after the jump occurs with two characteristic times. At short times the current decreases because of subsequent attachment (reaction (R1) of the laser photodetached electrons and some transient processes connected with changes in the discharge structure. At longer time scales, the current decreases due to ambipolar diffusion. The dynamics of the reduced electric field (figure 6(*b*)) supports these assertions. Further evidence of the reason for the initially fast current decay is provided by estimating the rate constant of the electron dissociative attachment to O_2 using the variation of fast decay data of discharge current after the laser pulse with pressure. As shown in figure 7, the estimated values of k_{att} are in reasonable agreement with the values calculated from the known cross-section [32] and the EEDF, obtained by solving Boltzmann's equation in the two-term approximation. Owing to the large error bars in the experimentally estimated rate constants, only the calculated values were used for further analysis.

In order to determine the fraction of negative ions photodetached by a laser pulse, the $[O^-]_{\text{pd}}/[O^-]_{\text{total}}$ ratio as a function of laser energy E_{las} is plotted in figure 8. The total concentration of negative ions can be obtained from the saturation value of this plot, as indicated by equation (6).

$$[O^-]_{\text{pd}} = O^- \left(1 - \exp\left(-\frac{E_{\text{las}}}{E_{\text{las}}^*}\right)\right), \qquad E_{\text{las}}^* = h\nu\frac{S}{\sigma_{\text{pd}}},$$
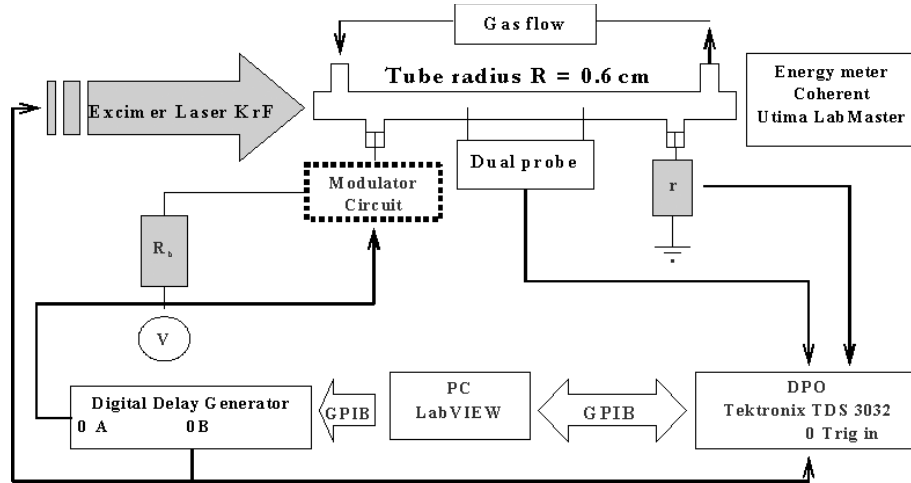
$$(6)$$

Figure 5. Schematic diagram of the laser photodetachment apparatus.
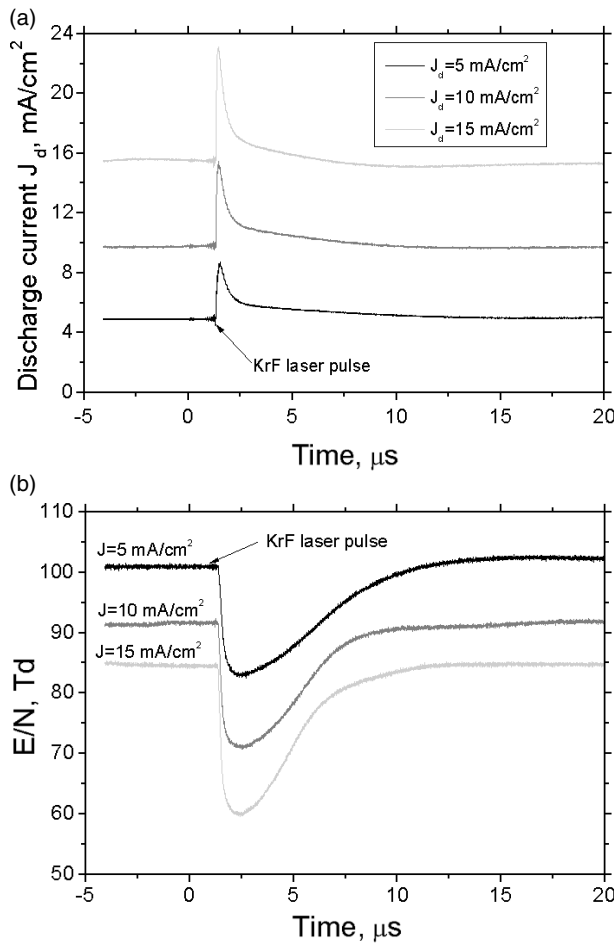

Figure 6. (*a*) Dynamics of discharge current after a laser pulse for different initial current densities. $p = 1$ Torr, energy of KrF laser, $E = 70$ mJ. (*b*) Dynamics of reduced electric field after a laser pulse for different initial current densities. $p = 1$ Torr, energy of KrF laser, $E = 70$ mJ.

Figure 7. Calculated (——) and experimentally estimated (data points) rate constant of dissociative attachment to O_2 as a function of E/N.

Figure 8. Normalized photodetachment signal as a function of laser power E_{las} at different discharge conditions.

where S—cross-section of the laser beam (the diameter of the laser beam was $d_{laser} = 0.9$ cm), $h\nu$—photon energy. Moreover, one can use the extracted value of the characteristic saturation energy E_{las}^* to obtain the so-called 'effective'
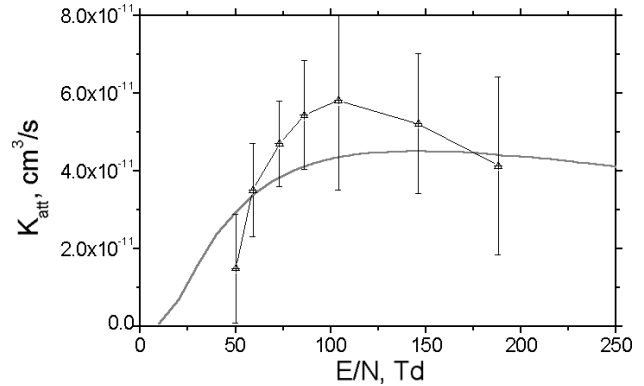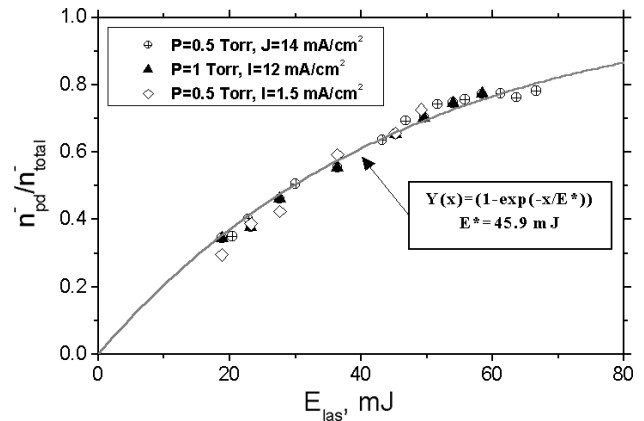
photodetachment cross-section as $\sigma_{pd} = (1.02 \pm 0.04) \times 10^{-17}$ cm^2. This value is in good agreement with the data for the O$^-$ absorption cross-section [33], suggesting that, under these conditions, O$^-$ is the main negative ion in the discharge and that the correct calibration procedures were applied.
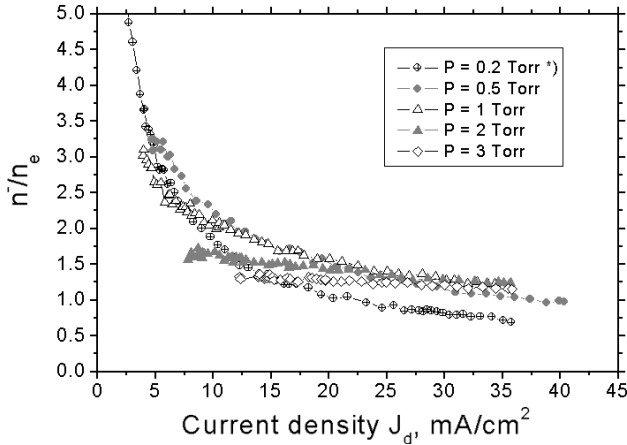
Figure 9. n^-/n_e ratio as a function of discharge current density J_d at different pressures in a stationary discharge.* The values of n^-/n_e at 0.2 Torr are underestimated (see discussion).

3. Negative ion concentration and dynamics

Results for negative ion concentration in stationary discharges are presented first. The n^-/n_e ratio (figure 9) decreases with increasing discharge current density (J_d), albeit at a slower rate at higher J_d. This is an indication that the concentration of species that destroys the negative ions increases with discharge current (or electron density), see also figures 3(*a*) and 4(*a*). Also, at very high currents, the concentration of these species saturates. These results are in agreement with equation (1).

Then, the negative ion dynamics was observed by time shifting the laser pulse with respect to the current modulation pulse and measuring the n^-/n_e ratio as a function of laser pulse delay. The time evolution of the n^-/n_e ratio, discharge current density J_d and reduced electric field E/N in a modulated discharge is presented in figures 10(*a*), (*b*) and (*c*), respectively, for two pressures: 'low'—0.2 Torr and 'high'—1.5 Torr. The initial fast jump of n^-/n_e and E/N, observed only at the low pressure (see figures 10(*a*) and (*c*)), is because the discharge is not in the attachment–detachment regime at such low pressure. Low pressure effects will be the subject of a separate investigation. Excluding this initial jump, the evolution of n^-/n_e, J_d and E/N displays two characteristic times. The first time constant turned out to coincide with the loss time of atomic oxygen, whereas the second coincided with the loss time of singlet molecular oxygen.

4. Discussion

In the pressure range investigated, the main source of negative ions is dissociative attachment of electrons to O_2 molecules (reaction (R1)). This has also been verified by our experiments. Besides O^- molecular negative ions O_2^- can also form in a low pressure oxygen discharge [18]. Important negative ion reactions are presented in table 1.

Two cases were realized in the experiments of this work: the 'high' pressure case corresponds to $pR > 0.3$ Torr cm. In this case, negative ion loss is dominated by associative detachment and the attachment–detachment regime of discharge operation is applicable. At such high pressure
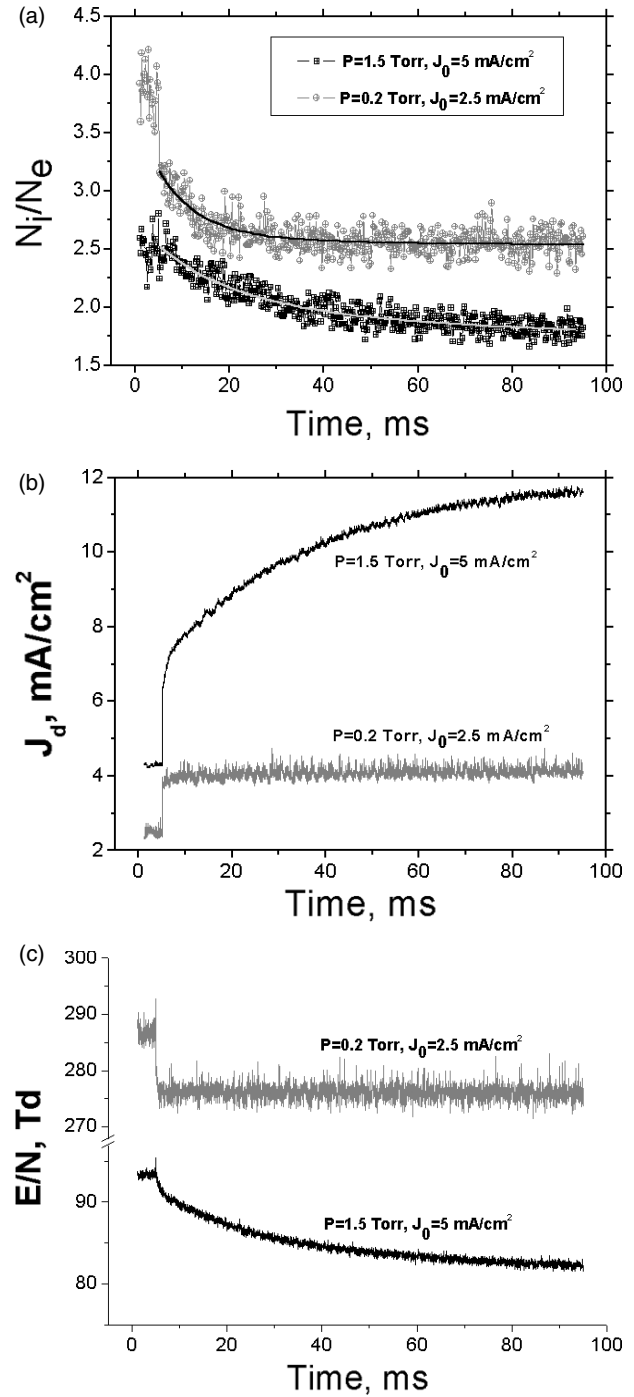

Figure 10. Dynamics of n^-/n_e ratio and fit using equation (1) (*a*), discharge current density J_d (*b*) and reduced electric field E/N (*c*) for modulated discharges at two pressures: 'low'—$p = 0.2$ Torr and 'high'—$p = 1.5$ Torr. The discharge current was switched at $t = 5$ ms.

there is no jump of either n^-/n_e or E/N at the moment of discharge current switching (see figures 10(*a*) and (*c*)). Both n^-/n_e and E/N vary smoothly with the characteristic times of evolution of atomic oxygen and singlet molecular oxygen. Since the degree of ionization is rather small ($<10^{-5}$), ion recombination (R6) and (R7) can be neglected, and the following expression for the total concentration of negative

Table 1. Most important reactions involving negative ions [14].

No	Reactions	Rate constants (cm³ s⁻¹)	This work (cm³ s⁻¹)
(R2)	$O^- + O \rightarrow e + O_2$	1.9×10^{-10} [15,16]	$(2.3 \pm 0.5) \times 10^{-10}$
(R3a)	$O^- + O_2(a\,^1\Delta_g) \rightarrow O_3 + e$	3×10^{-10} [15]; 0.33×10^{-10} [16]	$(1.9 \pm 0.4) \times 10^{-10}$
(R3b)	$O^- + O_2(a\,^1\Delta_g) \rightarrow O + O_2^-$	10^{-10} [18]	
(R4)	$O_2^- + O_2(a\,^1\Delta_g) \rightarrow 2O_2 + e$	2×10^{-10}	
(R5)	$O_2^- + O \rightarrow O^- + O_2$	3.3×10^{-10}	
(R6)	$O^- + O_2^+ \rightarrow O + O_2$	9.6×10^{-8}	
(R7)	$O_2^- + O_2^+ \rightarrow 2O_2$	4.2×10^{-7}	
(R8)	$O^- + O_2 \rightarrow O_2^- + O$	$f(E/N)$	
(R9)	$O_2^- + O \rightarrow O_3 + e$	1.5×10^{-10}	
(R10)	$O_2^- + O_2 \rightarrow 2O_2 + e$	$f(E/N)$	
(R11)	$O^- + O_2 \rightarrow O_2 + O + e$	$f(E/N)$	
(R12)	$O^- + O_2 \rightarrow O_3 + e$	$f(E/N)$	

ions ($n^- = [O^-] + [O_2^-]$) in the plasma volume can be written:

$$\frac{n^-}{n_e} = \frac{k_{att}(1 + ([O_2^-]/[O^-]))}{(k_2 - k_5([O_2^-]/[O^-]))X + (k_{3a} + k_{3b})Y + k_8 + k_{11} + k_{12}},$$

(7)

where

$$X = \frac{[O]}{[O_2]}, \qquad Y = \frac{[O_2(a\,^1\Delta_g)]}{[O_2]},$$

$$\frac{[O_2^-]}{[O^-]} = \frac{k_{3b}Y + k_8}{(k_5 + k_9)X + k_4Y + k_{10}}.$$

(8)

At high pressures, negative ion heating in the axial electric field is negligible as well, so processes (R8), (R10), (R11) and (R12) can also be neglected owing to the high threshold of these reactions. Since the fractions of atomic (X) and singlet oxygen (Y) are comparable under the experimental conditions, the O_2^- ion fraction turns out to be small, $[O_2^-]/[O^-] \approx k_{3b}/(k_5 + k_9 + k_4) \approx 0.05$–$0.14$. Indeed, in [18], O_2^- and O^- were measured separately in an RF discharge at $pR \sim 0.3$ Torr cm and the ratio $[O_2^-]/[O^-] \sim 0.1$. Neglecting k_8, k_{11} and k_{12}, and also neglecting the ratio $[O_2^-]/[O^-]$ compared with unity in the numerator, equation (7) becomes similar to equation (1), by replacing $k_{3a} + k_{3b}$ with k_3 and augmenting k_2 in equation (1) by $k_5([O_2^-]/[O^-]) \sim 0.3 \times 10^{-10}$ cm³ s⁻¹. It should be noted that, for the present experiments, the $pR > 0.3$ Torr cm regime corresponds to a pressure of $p = 0.5$ Torr. This is a transition pressure below which the effects of EEDF non-locality [24] and non-equilibrium ion diffusion [14] become important.

In the case of low pressure, when $pR < 0.3$ Torr cm (and $E/N > 200$ Td), negative ion heating becomes important. Then, charge transfer (R8) and negative ion losses in reactions with molecular oxygen ((R10), (R11), (R12)) can become significant. Moreover, at low pressures, the negative ion and electron radial concentration profiles are different (negative ions are trapped in the centre of the discharge by a strong ambipolar field), i.e. the discharge does not operate in the attachment–detachment regime any longer. Under these conditions, the n^-/n_e ratio near the discharge axis greatly exceeds the cross-section averaged value. Finally, O_2^- becomes the main negative ion instead of O^- (as shown in [14]). Therefore, the low pressure negative ion data obtained in this work should be analysed, taking into account

these complications. This will be the subject of a separate publication.

O_2^- ions may dominate at low pressures and low current densities in oxygen dc discharges as pointed out in [14]. At low pressures, O_2^- is produced mainly by charge exchange reactions (R3b and R8 in table 1), since tree-body attachment to O_2 is negligible ($k \sim 3.6 \times 10^{-31}$ cm⁶ s⁻¹). However, reaction (R3b) is compensated by reaction (R5). Thus, the significant process which may change the main negative ion from O^- to O_2^- is charge exchange with O_2 (reaction R8). Since this reaction has a threshold ($\varepsilon_{th} \sim 1$ eV), it is expected to be important only at high E/N, i.e. at low pressures.

All quantities in equation (1), except k_2, k_3 and k_{att}, were measured experimentally. The concentration of $[O_2]$ was obtained using the ideal gas law and the measured gas temperature, taking into account the oxygen dissociation and singlet oxygen density. The dissociative attachment rate constants k_{att}^X and k_{att}^Δ were calculated based on known cross-sections, [32, 34, 35], respectively, and the EEDF obtained by solving Boltzmann's equation in the two-term approximation. The cross-section for dissociative attachment to $O_2(a\,^1\Delta_g)$ [35] was normalized according to Phelps' [36] recommendation. The calculated rate constants were in agreement with the published data on k_{att}^X and k_{att}^Δ in pure oxygen. The remaining two rate constants, k_2 and k_3, were treated as fitting parameters. The fits are shown in figure 11 as a function of pressure. The rate constants were practically independent of current density, i.e. their variation with current density was smaller than the experimental error. Rate coefficients k_2 and k_3 tend to a constant value at higher pressure, for which equation (1), based on the attachment–detachment regime, is valid. Thus, the rate constant of negative ion detachment with $O(^3P)$ atoms ($O^- + O(^3P) \rightarrow O_2 + e$) is found to be $k_2 = k_d^O = (2.3 \pm 0.5) \times 10^{-10}$ cm³ s⁻¹, and that with $O_2(a\,^1\Delta_g)$ molecules ($O^- + O_2(a\,^1\Delta_g) \rightarrow$ products + e) is found to be $k_3 = k_d^\Delta = (1.9 \pm 0.4) \times 10^{-10}$ cm³ s⁻¹. The reported value of k_2 reflects an augmentation by 0.3×10^{-10} cm³ s⁻¹, as discussed earlier, to make equations (1) and (7) equivalent. The rising value of the rate constants at low pressure is connected with the complications referred to above. These low pressure values should be considered of no significance. Error bars in figure 11 reflect the statistical deviation of k_2 and k_3, obtained at different conditions (discharge current, ballast resistance, etc).

The obtained rate constant for detachment with oxygen atoms is in excellent agreement with the literature data (see
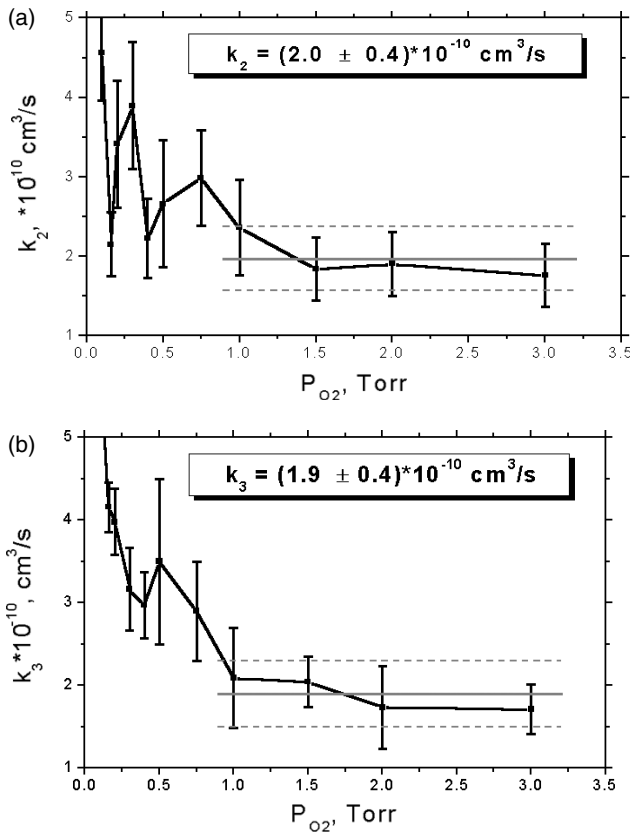
Figure 11. Rate constants k_2 (*a*) and k_3 (*b*), obtained by fitting the experimental data of n^-/n_e dynamics using equation (1).

table 1). The rate constant for detachment on singlet oxygen molecules k_d^Δ differs noticeably both from the generally accepted value [15] and from the rate constant measured in [16]. However, the authors of [15] pointed out that the reported value of k_d^Δ may be in error by as much as 100%, within the range of the value found in this work. In [16], the concentration of singlet molecules was measured before the reactor inlet. Accounting for a transport time up to the reactor inlet of 5 s, quenching on the tube walls (even for a very small value of $\sim 10^{-5}$ for the quenching probability) could have significantly decreased the concentration of singlet oxygen in the reactor. Overestimation of the $O_2(a\,^1\Delta_g)$ concentration leads to underestimation of the detachment rate constant. Thus, the value of k_d^Δ reported in [16] (0.33×10^{-10} cm^3 s^{-1}) should be considered a lower limit. In contrast to previous studies, in this work the rate constants of detachment with $O(^3P)$ atoms and $O_2(a\,^1\Delta_g)$ molecules were determined, for the first time, in the plasma itself. Moreover, negative ions, oxygen atoms and singlet molecules were all measured under the same conditions.

5. Conclusion

The dynamics of negative ion density in the positive column of a dc glow discharge in pure oxygen was investigated using laser photodetachment over a wide range of pressure (0.1–5 Torr) and current density (2–40 mA cm^{-2}). Using square wave modulation of the discharge current (switching time $\sim 0.25\,\mu$s), two time scales were observed in the negative ion dynamics: a 'slow' time scale of ~ 10 ms and a 'fast' time scale of $\sim 10\,\mu$s.

The fast ion density dynamics was observed only at pressures <0.5 Torr.

At higher pressures (>0.5 Torr), O^- negative ions are formed mainly by dissociative attachment of electrons to O_2 and are destroyed mainly by detachment from $O(^3P)$ and $O_2(a\,^1\Delta_g)$. It was revealed that O^- is the main negative ion in this attachment–detachment regime of discharge operation. Under these conditions, the radial profiles of negative ion density and electron density are similar, i.e. the density ratio is independent of radius and equal to the cross-section average value. In addition, $O(^3P)$ and $O_2(a\,^1\Delta_g)$ losses on the discharge tube walls occur in the kinetically controlled regime. Therefore, the concentration profiles of these species are identical to the profile of ground state molecular oxygen, as determined by the gas temperature profile. These facts allowed an investigation of the negative ion loss processes by reactions with $O(^3P)$ and $O_2(a\,^1\Delta_g)$ molecules in the plasma volume. The dynamics of the $O(^3P)$ concentration was investigated using time-resolved actinometry. The dynamics of the $O_2(a\,^1\Delta_g)$ concentration was measured using IR spectroscopy at $1.27\,\mu$m. Analysis of negative ion, oxygen atom and singlet oxygen molecule dynamics allowed determination of the rate constants of $O^- + O(^3P) \rightarrow O_2 + e$ ($k_d^O = (2.3 \pm 0.5) \times 10^{-10}$ cm^3 s^{-1}) and $O^- + O_2(a\,^1\Delta_g) \rightarrow$ products + e ($k_d^\Delta = (1.9 \pm 0.4) \times 10^{-10}$ cm^3 s^{-1}), in the plasma itself for the first time. In addition to these rate constants, measurements reported in this work (atomic oxygen density, singlet molecular density, loss probabilities of these species, gas temperature, negative ion density) as a function of discharge pressure and current density, provide a wealth of information which should be very useful to modelling studies of the oxygen discharge.

The 'fast' dynamics of the n^-/n_e ratio was observed only at low pressure (<0.5 Torr). In this case, ion heating in the strong electric field makes additional negative ion loss channels possible. Also, negative ions are strongly 'piled-up' near the discharge centre and the negative ion density profile is not similar to the electron density profile (the density ratio depends on radial position). Finally, the molecular ion becomes the dominant negative ion in the discharge. These complications dictate a different method of analysis of the low pressure data, which will be presented in another publication.

References

[1] Lieberman M A and Lichtenberg A J 1994 *Principles of Plasma Discharges and Material Processing* (New York: Wiley)
[2] Ramamurthi B and Economou D J 2002 *J. Vac. Sci. Technol.* A **20** 467–78
[3] Panda S and Economou D J 2000 *J. Appl. Phys.* **87** 8323–33
[4] Bogdanov E A, Kudryavtsev A A, Tsendin L D, Arslanbekov R R, Kolobov V I and Kudryavtsev V V 2003 *Tech. Phys.* **48** 1151–8

[5] Bogdanov E A, Kudryavtsev A A, Tsendin L D, Arslanbekov R R, Kolobov V I and Kudryavtsev V V 2003 *Tech. Phys.* **48** 983–94

[6] Oskam H J 1958 *Philips Res. Rep.* **13** 335

[7] Bogdanov E A, Kolobov V I, Kudryavtsev A A and Tsendin L D 2002 *Tech. Phys.* **47** 946–54

[8] Bogdanov E A and Kudryavtsev A A 2001 *Tech. Phys. Lett.* **27** 905–7

[9] Franklin R N 2002 *Plasma Sources Sci. Technol.* **11** A31–7

[10] Franklin R N 2001 *Plasma Sources Sci. Technol.* **10** 174–9

[11] Franklin R N 2000 *J. Plasma Phys.* **64** 131–53

[12] Franklin R N and Snell J 1999 *J. Phys. D: Appl. Phys.* **32** 2190–203

[13] Kolobov V I and Economou D J 1998 *Appl. Phys. Lett.* **72** 656

[14] Ivanov V V, Klopovskiy K S, Lopaev D V, Rakhimov A T and Rakhimova T V 1999 *IEEE Trans. Plasma Sci.* **27** 1279–87

[15] Fehsenfeld F C, Albritton D L, Burt J A and Schiff H I 1969 *Can. J. Chem.* **47** 1793

[16] Upschulte B L, Marinelli W J and Green B D 1994 *J. Phys. Chem.* **98** 837–42

[17] Touzeau M *et al* 1991 *J.Phys. D: Appl. Phys.* **24** 41

[18] Stoffels E, Stoffels W W, Vender D, Kando M, Kroesen G M W and de Hoog F J 1995 *Phys. Rev.* E **53** 2425–35

[19] Hayashi D and Kadota K 1998 *J. Appl. Phys.* **83** 697–702

[20] Katsch K M, Sturm T, Quandt E and Dobele H F 2000 *Plasma Sources Sci. Technol.* **9** 323–30

[21] Lopaev D V and Smirnov A V 2004 *Plasma Phys. Rep.* **30** 882–93

[22] Klopovskiy K S, Lopaev D V, Popov N A, Rakhimov A T and Rakhimova T V 1999 *J. Phys. D: Appl. Phys.* **32** 3004–12

[23] Ivanov V V, Klopovskiy K S, Lopaev D V, Rakhimov A T and Rakhimova T V 2000 *Plasma Phys. Rep.* **26** 980–90

[24] Ivanov V V, Klopovskiy K S, Lopaev D V, Rakhimov A T and Rakhimova T V 2000 *Plasma Phys. Rep.* **26** 972–9

[25] Klopovskiy K S, Lopaev D V, Proshina O V, Rakhimov A T and Rakhimova T V 2004 *Plasma Phys. Rep.* **30** 542–8

[26] Pagnon D, Amorim J, Nahorny J, Touzeau M and Vialle M 1995 *J. Phys. D: Appl. Phys.* **28** 1856

[27] Boffard J B, Lin C C and DeJoseph C A Jr 2004 *J. Phys. D: Appl. Phys.* **37** R143–61

[28] Malyshev M V and Donnelly V M 1997 *J. Vac. Sci. Technol.* A **15** 550–8

[29] Lopaev D V and Smirnov A V 2002 *Proc. 3rd Int. Symp. on Theoretical and Applied Plasma Chemistry (ISTAPC-2002) (Plyos, Russia)* vol 1, pp 213–16

[30] Newman S M, Lane I C, Orr-Ewing A J, Newnham D A and Ballard J 1999 *J. Chem. Phys.* **110** 10749

[31] Newman S M, Orr-Ewing A J, Newnham D A and Ballard J 2000 *J. Phys. Chem.* **104** 9467

[32] Itikawa Y, Ichimura A, Onda K, Sakimoto K, Takayanagi K, Hatano Y, Hayashi M, Nishimura H and Tsurubuchi S 1989 *J. Phys. Chem. Ref. Data* **18** 23

[33] Jinno M, Kubo M, Aono M and Itatani R 1997 *Japan. J. Appl. Phys.* **36** 2870–3

[34] O'Malley T F and Taylor H S 1968 *Phys. Rev.* **176** 207

[35] Belic D S and Hall R I 1981 *J. Phys.* B **14** 365–73

[36] Phelps A V private communication, ftp://jila.colorado.edu/collision_data/